

Merci

Measurement Error and Correlation Impact on the Atmospheric Dynamics Mission

Draft Task 2 report

ESA Reference: FS/0304/PI/pi, version 1.1 (RFQ/3-9992/01/NL/MM)

Ad Stoffelen, KNMI
Måns Håkansson, MISU
Gert-Jan Marseille, KNMI

Prime contractor:

Ad Stoffelen, WM-SD, KNMI.
Postbus 201
3730 AE de Bilt
The Netherlands

Tel: +31 30 22 06 585
Fax: +31 30 22 10 407
E-mail: Ad.Stoffelen@KNMI.NL

Associate:

Erland Kallen
Dept. of Meteorology, Stockholm University
Arrhenius Laboratory
SE-106 91 Stockholm
Sweden
Tel: +46 8 162396 ; Fax: +46 8 15 71 85
E-mail: erland@misu.su.se

Approved by:

Dr. Sylvia Barlag
Head of Satellite Data section,
Observations and Modelling Dept., KNMI

Dr. Ir. Ad Stoffelen
Project Manager, Satellite Data section,
Observations and Modelling Dept., KNMI

Date: 11 October, 2002

Table of Contents

1	INTRODUCTION	1
1.1	Reference documents	1
1.2	Accuracy Requirements	1
1.2.1	Error Correlation	2
1.2.3	Observations and Measurements and their Errors	4
1.2.4	Atmosphere	6
1.3	Evaluation of Tasks 1a and 1b	7
2	Performance Analysis Tool and Data Bases	8
2.1	Performance Analysis Tool	8
2.1.1	LIPAS	8
2.1.2	LIPAS update	9
2.1.3	Wind Representativeness Errors	9
2.1.4	Error structure analysis	14
2.2	Data Bases	18
2.2.1	Mesoscale Wind Variability	18
2.2.2	Influence of Humidity on Aerosol Scattering Properties	20
2.2.3	Data Base Construction	24
2.3	Error Scenarii	25
2.3.1	Error Covariances	25
2.3.2	Wind Calibration	26
2.3.3	Temperature Effects	27
2.3.2	Proposed Error Scenarii	27
3	Conclusions	28
4	References	29
	Acronyms	32

1 INTRODUCTION

The MERCI proposal was submitted to ESA/ESTEC by the Royal Netherlands Meteorological Institute (KNMI), following ESA's Statement of Work (SoW) FS/0304/PI/pi, version 1.1, titled: "The Impact of Measurement Errors and their Correlation on the Atmospheric Dynamics Mission (ADM-Aeolus)", associated with RfQ 3-9992/01/NL/MM.

A team consisting of KNMI, DNMI, LMD, MISU, and SMHI has been assembled, supported by experts from Météo-France (MF) and by Michael Vaughan.

This Task 2 report describes the contributions of KNMI and MISU.

1.1 Reference documents

The following documents are referenced:

- 1 MERCI proposal to ESA
- 2 Task 1a report
- 3 Task 1b report

1.2 Accuracy Requirements

The World Meteorological Organisation (WMO) published documents on the capabilities of the current Global Observing System (GOS) and the requirements for improving meteorological analyses (WMO, 1996, 1998, 2000). It is stated in these documents that for wind profile data temporal and spatial coverage is lacking in the current GOS and GCOS. Requirements are given for quality and quality which have lead to the requirements set for the ADM (see ESA, 1999). However, these WMO publications do not provide a clear guidance on the spatial error characteristics, whereas, from experience in the application of particularly passive sensor satellite observations in numerical meteorological analysis, it is well-known that the spatial error characteristics can be of crucial importance. With this in mind a strict error correlation requirement has been set for ADM of 0.01 (ESA, 1999).

The potential users of DWL observations are dealing with error correlation for existing observing systems e.g. radiosondes or radar wind profilers. The main requirement is related to the accuracy on the knowledge (a priori) of the measurement error covariance matrix that is used in the analysis equations for assigning the appropriate weight to observations. A priori means before using the observations in the meteorological state analysis, i.e., before any observation system is used, its error characteristics are determined as accurately as possible by comparison to the meteorological model and to other observation systems. In this way, error properties are determined that are often unknown to the instrument experts but essential a priori knowledge for the use of the observations (e.g., Stoffelen, 1998, chapters II, III, IV, and Appendix A). In

addition, users can perform calibration if biases are fixed (and unknown), or vary in a known way (with undetermined amplitude), for example as a function of orbit phase.

The horizontal line-of-sight (HLOS) wind observation bias or systematic error is also included in the error covariance matrix formalism but is specified to be small (presently bias < 0.1 m/s; see ESA, 1999). The variances of the random errors (the square of the HLOS wind observation accuracy) are represented by the diagonal terms of the error covariance matrices. The HLOS wind observation accuracy is specified to be better than 1 m/s between 0 and 2 km and better than 2 m/s between 2 and 16 km (cf. Annex A of SoW).

No requirement to limit correlated errors over altitude bins has been formulated yet but the wind observation error must meet the overall requirements under strongly varying signals from one bin to the next, as the atmospheric model prescribed to verify the instrument performance does include for example a high cirrus cloud. The frequency and distribution of occurrence of such cases needs to be investigated further to estimate their relevance on performance.

1.2.1 Error Correlation

To study temporal and by consequence spatial correlation of error the following definitions are used. Suppose we have a data base defining the true atmospheric state denoted by vector \mathbf{t} . \mathbf{t} contains profiles of relevant atmospheric variables, such as the west-east and north-south wind components u and v , cloud liquid water content CLW , aerosol loading, etc.. For example, \mathbf{t} contains realistic distributions of coherent wind structures. ALADIN can be characterised by a vector \mathbf{I} , containing instrument variables such as laser energy E , wavelength λ , telescope diameter D , receiver bandwidth B , etc.. An ALADIN observation f_i of the LOS wind t_i can then be characterised by

$$f_i = t_i + \delta_i \quad (1)$$

where

$$\delta_i = \delta_i(\mathbf{t}, \mathbf{I}) \quad (2)$$

is the error of the observation depending on the atmospheric state and the instrument. For two observations i and j we define error covariance by

$$O_{ij} = \langle (f_i - t_i)(f_j - t_j) \rangle = \langle \delta_i \delta_j \rangle \quad (3)$$

and error correlation by

$$\rho_{ij} = \frac{O_{ij}}{\sqrt{O_{ii} O_{jj}}} \quad (4)$$

For example, suppose a receiver gain bias of 10% by $\alpha = 0.1$ and

$$\begin{aligned}
 f_i &= (1 + \alpha)(t_i + \delta_i^t); \\
 \delta_i &= \alpha t_i + (\alpha + 1)\delta_i^t; \\
 O_{ij} &= \alpha^2 \langle t_i t_j \rangle, i \neq j \\
 O_{ii} &= \alpha^2 \langle t_i^2 \rangle + (\alpha + 1)^2 \langle \delta_i^{t^2} \rangle
 \end{aligned} \tag{5}$$

such that after assuming that the expected "true" error variabilities δ_i^t and δ_j^t , for example mainly determined by photon count statistics, are of the same size and uncorrelated as well as assuming uniform wind variability, i.e., $O_{ii} = O_{jj}$ we get

$$\rho_{ij} = \frac{\langle t_i t_j \rangle}{\langle t_i^2 \rangle + \left(1 + \frac{1}{\alpha}\right)^2 \langle \delta_i^{t^2} \rangle}, \quad i \neq j \tag{6}$$

Note that this correlated error has the spatial structure of the wind field itself through $\langle t_i t_j \rangle$, i.e., the structure of the wind field as sampled by the instrument, and is thus flow dependent. Obviously, many other types of error equations exist and we propose here to formulate the most relevant ones for ADM.

It must be strange for an external reader that the first task envisaged here is called "definition of the term error correlation". The term is perfectly defined above, but what we are really after is the definition of the probability space; in other words, the question is

ON WHAT TYPES OF MEASUREMENT SAMPLES MUST THIS ERROR CORRELATION BE COMPUTED?

Having stated in the requirements that the ADM winds should not be substantially affected by any error correlation, it is obvious that

1. If the samples used to estimate this correlation are too big (such as involving all the data over the whole globe, all seasons, then all air masses, strong jets as well as calm winds, etc...), then the above-quoted requirement is likely not stringent enough; but
2. If the samples used to estimate this correlation are too small (such as only the wind measurements obtained in a jet core exceeding 100m/s in 3h on one given day), then this correlation requirement is too stringent.

The second phase of this task includes the definition of some meteorological data samples on which the spatial correlation requirement must apply. We propose here to quantify error correlation requirements for wind profiles on given atmospheric data sets t .

What should be definitely avoided are errors that are very dependent on the flow or the air-mass. These would lead to non-negligible error correlation on measurement samples covering typically atmospheric volumes 1000km x 1000km x 5km (orders of magnitudes). If we have for example a jet-stream whose size is around 2000km x 300km x 1km, and if all the wind measurements in this jet are underestimated by a few m/s when the flow is higher than 30m/s, this is quite unacceptable. This is the typical "old" cloud motion wind observation problem. On

the other hand, if the same problem occurs only above 100m/s, leading to 3 ALADIN measurements (close to each other) to have the same observational error of -2m/s (-2% then), then this is quite acceptable even if it may lead to a 100% error correlation when computed on such small sample size.

Calibration problems can be very detrimental. For example, using ERS scatterometer wind data, ECMWF at some point changed their boundary layer winds such that ERS was biased 10% low. Then they noticed negative impacts from the ERS winds. After taking away this 10% difference the ERS wind impacts became positive again. In case of the ERS scatterometer we can take away these 10% because the instrument is (very) stable in time. If the number (10%) would vary along an orbit in an unpredictable way then we are really lost and are exposed to negative impacts all the time! See also equation (6).

The ERS calibration problem above is an example of a flow-dependent error. Similarly for ALADIN, if the true component wind distribution has a standard deviation of 20 m/s, then a receiver gain bias of 10% results in an expected 2 m/s uncertainty. It appears as a spatially coherent error since the atmospheric flow itself is correlated on scales of several hundreds of km horizontally and typically a km vertically. As mentioned, such errors really can destroy the capability to measure realistic atmospheric wind variability.

However, note that in equation (6) $\langle t_i t_j \rangle$ is only non-zero if the locations i and j are closeby; over a global set of winds $\langle t_i t_j \rangle \cong 0$ and **no apparent calibration problem** will be noted over such a data set, even though the instrument may be **useless**.

We propose to perform parametric instrument simulations to understand how the ALADIN measurements and their processing would react on various types of air-masses and atmospheric flows. In other words, we will effectively vary the instrument vector \mathbf{I} for a to be determined relevant set of atmospheric scenarios \mathbf{t} , in order to assess compatibility with the wind profile observation error structure requirements. This will allow ESA to refine the ALADIN instrument requirements on temporal error correlation.

1.2.3 Observations and Measurements and their Errors

In the case of ALADIN up to 50 pulses are accumulated on the detector for each **measurement** and are down-linked. These determine the wind measurement signal and noise characteristics for a particular altitude bin resolved by range-gating. These Doppler shift measurements will then be integrated by an on-ground processing scheme to result in a wind **observation** over 50 km. This means, that, on average, 10 or more measurements are combined on-ground to obtain one observation. Two subsequent wind observations are separated by 200 km in accordance with the observational requirements as summarised in Table A.1 of Annex A of the RfQ SoW.

Figure 1 provides an example of such sampling using the LITE UV backscatter lidar. It is clear that due to the ADM sampling information on relevant atmospheric properties is lost. It is worthwhile to investigate the associated error properties of the DWL profile measurements and observations.

The backscatter over the altitude range of interest (26 km) from an individual laser pulse is received within 200 μ s. Two adjacent range gates of this pulse are about 3 μ s apart. Over these time scales, the thermal environment is assumed to be stable. Also pointing variations of the spacecraft are expected to be negligible. Thus the only effects leading to an error correlation in a backscatter signal result from effects in the receiver chain. On the Rayleigh and Mie receiver chains the signal is accumulated in each altitude bin over a period of up to 0.5 s.

During the on-board accumulation, time errors in sampling the backscattered light can lead to error correlation between various altitude bins. This effect can be controlled by instrument design. In particular, the orbit altitude can vary during a wind observation by over 100 m, which could lead to some correlation of wind errors over adjacent altitude bins. In a common wind shear case of 4 m/s per km, this would lead to an error correlation of 0.4 m/s between neighbouring height levels. Note that such error is flow (shear) dependent. As such, this altitude variation must be compensated for by ADM. RMS geometric height assignment is required to be below 50 m (see Annex A of RfQ SoW).

The receiver chain may exhibit radiometric and spectral impurities or uncertainties that could give rise to spatially correlated measurement error when these artefacts appear over periods longer than 10 μ s (vertical) or 0.5 s (horizontal).

Longer-term correlation resulting from temperature drifts induces zero-wind bias and gain errors. This bias has been tentatively specified to stay below 0.1 m/s over the time between two zero-wind calibrations. Gain stability has not been specified yet, and gain drifts have so far only been considered as a term in the overall velocity accuracy budget. We note that gain drifts affect the observation of the vertical wind shear (variability) in the same way as they affect the wind itself (from equation 5). Wind shear is one of the major causes of instability in the atmosphere. It may be clear that a systematically wrong observation of shear could cause the lidar data to detrimentally affect atmospheric analysis. We therefore propose to specifically address wind shear observation performance in this study.

Gain stability is the parameter that industry understands very well, and that the users can translate into an uncertainty of measuring certain particular wind variabilities, such as jets. In fact, we just need gain prediction accuracy within the total HLOS error of 2-3 m/s up to 100 m/s. At 100 m/s we may for instance allow half the error to be systematic (gain). The gain knowledge should then be about 1%. We propose to further study these numbers.

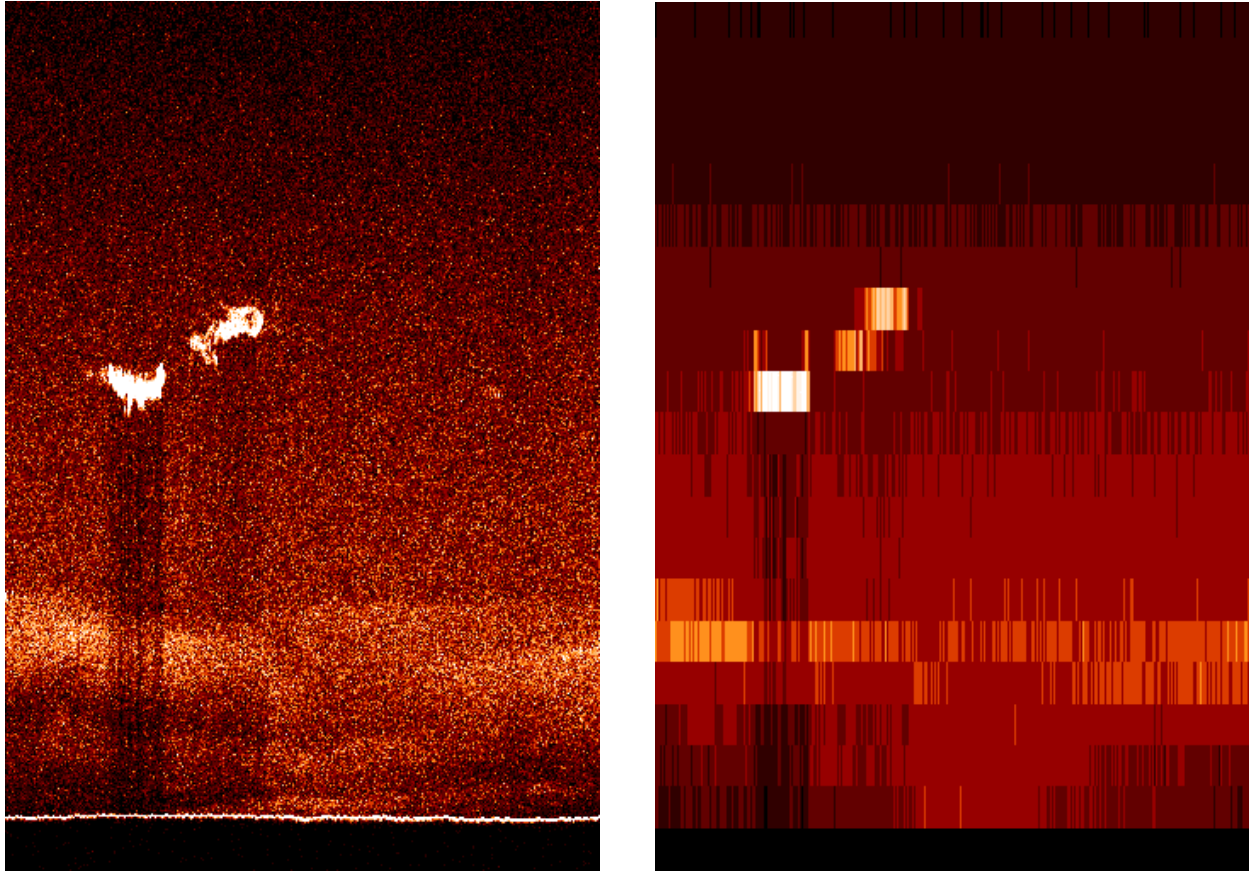


Figure 1: LITE UV backscatter measurements at full resolution (left) and at a resolution compatible with the ADM (right) measurements over a period of about 10 s. Cloud and aerosol structure that modulate the ADM signal are clearly lost by the ADM sampling giving rise to uncertainty in the interpretation, e.g., signal height assignment.

1.2.4 Atmosphere

The atmospheric frequency response is a convolution of the backscatter profile and the LOS speed of the air mass over a range gate. Atmospheric stratification will result in a mean signal height different from the geometric mean height. This difference or error can be correlated between neighbouring measurements when an aerosol or cloud layer extends over more than one range gate (e.g., see figure 1). Similarly, during the on-board accumulation, a change of the altitude of scattering layers can lead to error correlation between neighbouring altitude bins.

Another effect obvious from figure 1 is the change of height of aerosol layers from one measurement to its neighbour. If wind variability patterns are associated to these changes in aerosol stratification then errors in height assignment of such neighbouring measurements may be correlated horizontally, but at the same time vertically. Note that both mentioned height assignment problems are probably most acute for the Mie channel return, but that it could also cause problems in the Rayleigh channel due to associated variations in the transmission profile.

These effects are dependent on the meteorological scene and the magnitude and frequency of occurrence need to be assessed in more detail using numerical performance simulations in this study. In a preliminary assessment Lorenc et al (1992) concluded that the spatial wind variability over vertical scales of 1 km and smaller is generally much less than the spatial wind variability over horizontal scales smaller than 50 km. This would indicate that vertical stratification problems are of less relevance than the atmospheric variability in the horizontal.

In for example clear air turbulence or orographic wave activity more extreme atmospheric variabilities are expected (Lorenc et al, 1992), but it is anticipated that such cases can be identified in the DWL measurements and quality control rejection may be applied. This hypothesis needs to be checked carefully.

Coherent structure in atmospheric variability may be particularly pronounced in the presence of clouds. At the same time, our knowledge about the circulation in cloudy regions is generally the most limited and any observation is welcome to improve our knowledge. Investigation of the detailed microphysical structures around clouds is clearly beyond the scope of this study. What we propose is to investigate the consequences of the increased signal variability in scenes with clouds in terms of reduced accuracy and anticipated error structure.

1.3 Evaluation of Tasks 1a and 1b

Task 1a briefly describes the potential errors and its correlation related to the platform, instrument, and atmospheric conditions, of the ADM observations. Possible scenarii of error are summarised. These will be further considered here.

Task 1b provides an overview of the experience and practise in the NWP community with respect to detrimental effects with respect to observation error and error correlation. An equation is provided to analyse the effects of unknown observation error. Error correlation in the vertical on the km scale and horizontal error correlation on the synoptic scale seem most damaging. Meteorological cases that are critical to forecast due to a lack of observations are provided for reference. Conclusions are:

- Much experience exists with respect to correlated observations, and in particular errors on the synoptic scale in the horizontal and km-scale in the vertical are known to be detrimental; these detrimental effects of correlated data are supported by theoretical computations;
- If the nature of the bias is known, bias correction or data thinning are effective means to limit detrimental effects;
- So-called randomly correlated observation errors are most damaging; theoretical evidence shows that due to such errors information on atmospheric spatial structures is lost;
- Critical cases present usually air masses with strong space and time variations, where the model forecasts are very sensitive to the initial state (analysis). A lists of such cases has been provided.

In task 2, we take the suggested scenarios from Task 1a and the analysis of Task 1b in order to design a parametric simulation and analysis tool for studying the possible detrimental effects of errors on the ADM-Aeolus mission objective of providing accurate wind field analyses. Suitable data bases are constructed in order to investigate several error scenarii.

2 Performance Analysis Tool and Data Bases

2.1 Performance Analysis Tool

Task 2a of the Measurement ERror Correlation Impact (MERCi) study includes the definition of a simulation tool to simulate realistic horizontal line-of-sight (HLOS) wind observation errors and a scheme to analyse observation error structures (correlations). In Task 3 this scheme is implemented, tested, and these structures are further analysed to assess their possible detrimental effects on meteorological analyses.

Part of the Lidar Performance Analysis Simulation (LIPAS) tool developed at KNMI (Veldman, 1999), that simulates the performance of the ADM phase-A Doppler wind lidar (DWL), will serve as the basis for simulating observation error structures. The main components of LIPAS are shortly outlined in the next section. Limitations of LIPAS and modifications are discussed in section 1.3. A scheme to analyse observation errors as produced by the updated LIPAS tool is discussed in section 1.4.

2.1.1 LIPAS

The Lidar Performance Analysis Simulation (LIPAS) tool has been developed by KNMI and NLR (National Aerospace Laboratory) to simulate the expected performance of a DWL attached on the International Space Station. KNMI participation included all aspects of the phase-A DWL (ESA, 1999), i.e. emission of laser light, interaction of emitted laser with atmospheric particles, detection of the backscattered light and post-processing to retrieve HLOS wind components. The software was written in FORTRAN77 and can be executed independently from the advanced simulation tool developed at NLR.

The simulator includes realistic atmospheric conditions, including winds, clouds and humidity from the ECMWF OSSE database nature run (Stoffelen, 1994) and temperature and air density profiles from a climatological database. Aerosol (cloud) backscatter and extinction at 0.355 micron laser wavelength are derived from statistics of aerosol backscatter at 10.6 micron, as obtained from measurement extensive campaigns in the Atlantic around 1990, and by using a backscatter scaling law (Vaughan, 1998). LIPAS will be extended to incorporate additional atmospheric databases as provided by the user.

LIPAS includes the lidar concept as proposed in Phase-A. It includes the Mie multi-channel technique to retrieve HLOS wind velocities from detected light backscattered from aerosols and the Double-edge technique to retrieve winds from molecular returns. Signal accumulation over a distance of 3.5 km (i.e. 0.5 seconds or 50 shots) has been implemented. A single observation is retrieved from 14 accumulations. For non-cloudy profiles the accumulations are simply

averaged. In cloudy scenes, a number of accumulations contain cloud, depending on cloud cover and by using a random number generator. These accumulations are processed separately. LIPAS includes the ECMWF cloud overlap model to simulate cloud cover in adjacent atmospheric layers.

The output of LIPAS is a profile of HLOS winds and random error characteristics, ranging from the surface up to 20 km altitude with 1 km resolution. The random error is a superposition of instrument and representativeness errors that are both modeled as Gaussian distributions. Instrument errors are closely related to the SNR of the detected signal on the instrument receiver and processing steps to retrieve the frequency shift and HLOS wind velocity component. A fixed profile of representativeness errors as a function of pressure level (Lorenc, 1992) has been implemented in LIPAS.

2.1.2 LIPAS update

LIPAS ignores horizontal aerosol backscatter variability within an observation. Moreover, a uniform aerosol distribution within a range gate is assumed. LIPAS is updated to include aerosol backscatter variations both in the horizontal and vertical. Results from the LITE4ADM project, running parallel with MERCI at KNMI, and aiming at aerosol backscatter retrieval from the LITE database will be used to study effects of spatial aerosol variability.

HLOS wind profile resolution has been constrained to 1 km. LIPAS will be updated to become more flexible for user-specified resolutions.

The error formulation of Task 1a, Eq. (1.13) will be adopted in LIPAS. Initially, we will focus on some of the proposed error scenarios, i.e. *i*) the simple velocity dependent bias, linear and quadratic, to study gain biases, *ii*) the simple orbit bias, assuming a higher harmonic orbit variation and *iii*) vertical shifts of the complete profile due to errors in the range gate localisation.

2.1.3 Wind Representativeness Errors

The updated LIPAS must be able to analyse HLOS wind error structures for typical meteorological cases. The input will be a characterization of the atmospheric conditions as a sample of profiles of wind, temperature, specific humidity, cloud cover, cloud liquid water/ice content and aerosol backscatter. These profiles are provided at a user specified resolution and interpolated inside LIPAS to ADM resolution. Next, LIPAS simulates sampling of the atmosphere by the ADM-DWL. For each sample input, the output of LIPAS will be a “true” HLOS wind profile, from the “true” input wind profile, and a HLOS wind profile including additional errors. The sample of true and measured HLOS wind profiles are archived and will serve as input for task 3 to identify structures (correlations) in the error statistics.

The next subsection provides a theoretical discussion on HLOS wind observation error as implemented in LIPAS. As an example it describes the computation of error correlations from LIPAS output by means of a statistical analysis in case of aerosol stratification.

2.1.3.1 HLOS wind observation error

We consider the wind inside a grid box, the wind at laser shot location and the wind as observed by a lidar

1. True wind in grid box

$\underline{W}_T = (u_T, v_T, w_T)$: true 3-D wind in grid box

$\bar{W}_T = (\bar{u}_T, \bar{v}_T, \bar{w}_T)$: mean wind vector in grid box

$$\begin{aligned}\bar{u}_T &= \frac{1}{V} \int_{\text{grid box}} u_T(x, y, z) dV \\ \bar{v}_T &= \frac{1}{V} \int_{\text{grid box}} v_T(x, y, z) dV \\ \bar{w}_T &= \frac{1}{V} \int_{\text{grid box}} w_T(x, y, z) dV\end{aligned}$$

For the mean true HLOS wind component, w_{HLOS}^T in the grid box we then have

$$w_{\text{HLOS}}^T = -\bar{u}_T \sin(\psi) - \bar{v}_T \cos(\psi) \quad (7)$$

with ψ the azimuth angle, i.e. the angle (clockwise) between the laser beam direction and the geographical North. The ADM lidar aims at measuring this meteorological wind parameter.

2. True wind at laser shot location

$\underline{W}_L = (u_L, v_L, w_L)$: true local 3-D wind at shot location

The measured LOS wind component by the instrument, w_{LOS}^L , is the projection of the true local wind vector on the laser beam direction. This component may be split in two parts.

$w_{\text{LOS}_h}^L = [-u_L \sin(\psi) - v_L \cos(\psi)] \sin(\theta)$: the projection of the *horizontal* wind along the laser LOS

$w_{\text{LOS}_v}^L = w_L \cos(\theta)$: the projection of the *vertical* wind component along the laser LOS

with θ the local incidence angle.

$$w_{\text{LOS}}^L = w_{\text{LOS}_h}^L + w_{\text{LOS}_v}^L \quad : \text{ measured LOS wind component}$$

The projection of the measured LOS wind component onto the horizontal plane provides the horizontal line-of-sight wind component, w_{HLOS}^L :

$$\begin{aligned} w_{\text{HLOS}}^L &= w_{\text{LOS}}^L / \sin(\theta) \\ &= \frac{[-u_L \sin(\psi) - v_L \cos(\psi)] \sin(\theta) + w_L \cos(\theta)}{\sin(\theta)} \end{aligned} \quad (8)$$

The difference between w_{HLOS}^L and w_{HLOS}^T is the sum of the representativeness error, which corresponds to the wind variability within the grid box, and the error due to ignoring the vertical wind.

Note: LIPAS will be updated to include HLOS wind errors due to vertical wind.

3. Retrieved wind by DWL

The atmospheric return signal from a range gate of length R is integrated on the instrument. The wind velocity and aerosol backscatter distribution will in general not be uniformly distributed within the range gate.

$\beta_a(L, z)$: aerosol backscatter profile at shot location as a function of altitude z

The retrieved wind velocity for a particular range gate, indicated with superscript m , is related to the mean frequency shift of all photons detected due to the backscattered signal from within that range gate. Mathematically, the retrieved HLOS wind velocity is a weighted average of the HLOS wind velocity profile and the aerosol density profile:

$$w_{\text{HLOS}}^m = \frac{\frac{1}{R} \int_R \beta_a(L, z) w_{\text{HLOS}}^l(z) dz}{\int_R \beta_a(L, z) dz} \quad (9)$$

Example

For uniform aerosol backscatter $\beta_a(L, z) \equiv \beta_a$, we have for the retrieved HLOS wind

$$\begin{aligned}
 w_{HLOS}^m &= \frac{\frac{1}{R} R \beta_a \int_R w_{HLOS}^l(z) dz}{R \beta_a} \\
 &= \frac{1}{R} \int_R w_{HLOS}^l(z) dz \\
 &= \overline{w_{HLOS}^l}
 \end{aligned} \tag{10}$$

i.e. the range gate mean HLOS wind component at laser shot location.

–

Generally, aerosol backscatter will not be uniformly distributed within a range gate causing an error since the retrieved HLOS wind velocity component at the laser shot location expressed in Eq. (10) will differ from the mean HLOS wind velocity on the right hand side.

Note: LIPAS will be updated to include non-uniform aerosol backscatter.

4. Shot accumulation

In the ADM concept, the atmospheric return signals from N laser shots are accumulated on the instrument receiver. Instrumental errors, denoted ε , give an error on the retrieved horizontal LOS wind, w_{HLOS} .

$$w_{HLOS} = \frac{1}{N} \sum_{i=1}^N w_{HLOS}^m(i) + \frac{\varepsilon}{\sin(\theta)} \tag{11}$$

LIPAS assumes Gaussian distributed random instrument errors with standard deviation determined by the SNR of the detected signal and post-processing algorithms to retrieve the HLOS wind velocity.

A HLOS wind observation, w_{HLOS}^o is retrieved from K accumulations:

$$w_{HLOS}^o = \frac{1}{K} \sum_{k=1}^K \left\{ w_{HLOS}(k) + \frac{\varepsilon(k)}{\sin(\theta)} \right\} \tag{12}$$

Finally, the HLOS wind observation error, ε_θ , equals

$$\varepsilon_0 = w_{\text{HLOS}}^T - w_{\text{HLOS}}^o \quad (13)$$

Example

- Assume zero vertical wind velocity in the grid box, $w \equiv 0$.
- Assume uniform aerosol backscatter inside the grid box, $\beta_a(L, z) \equiv \beta_a$.

We then have from (10), (11) and (8) using $w \equiv w_L \equiv 0$

$$\begin{aligned} w_{\text{HLOS}} &= \frac{1}{N} \sum_{i=1}^N \bar{w}_{\text{HLOS}}^l(i) + \frac{\varepsilon}{\sin(\theta)} \\ &= \hat{w}_{\text{HLOS}}^l \\ &= -\hat{u}_L \sin(\psi) - \hat{v}_L \cos(\psi) + \frac{\varepsilon}{\sin(\theta)} \end{aligned} \quad (14)$$

with the hats denoting that the winds have been averaged over the accumulation length. Next, for w_{HLOS}^o we have from (12)

$$w_{\text{HLOS}}^o = [-\tilde{u} \sin(\psi) - \tilde{v} \cos(\psi)] + \frac{1}{K \sin(\theta)} \sum_{k=1}^K \varepsilon(k) \quad (15)$$

with the wiggles denoting wind velocity averaging over accumulations. For the HLOS wind observation error, using (13) and (7) we then have

$$\varepsilon_0 = [-(\bar{u}_T - \tilde{u}) \sin(\psi) - (\bar{v}_T - \tilde{v}) \cos(\psi)] + \frac{1}{K \sin(\theta)} \sum_{k=1}^K \varepsilon(k) \quad (16)$$

The first term is the representativeness error, the second term denotes the instrument error.

–

Equation (10) is the status of HLOS wind error computation in LIPAS before the proposed update. The instrument error, ε , is a function of the SNR of the detected signal on the telescope receiver and inaccuracies in the post-processing step to retrieve the LOS wind from the detected signal. In LIPAS, a fixed profile of representativeness errors as a function of pressure level has been implemented (Lorenc, 1992). Both instrument and representativeness errors are assumed Gaussian.

To quantify expected error correlations using LIPAS in Task 3, we need a more realistic description of the instrument errors, making use of Task 1a output and realistic non-uniform aerosol backscatter distributions. The latter may be obtained from the MISU study to retrieve

aerosol backscatter from humidity profiles, Task 2b, and also, results from the LITE4ADM project can be used. Output from the mesoscale variability study in Task 2b is required to better quantify representativeness errors for the particular case under study.

LIPAS will be applied to samples of user-supplied atmospheric profiles. Vertical error correlations will be quantified in Task 3b from a statistical analysis of errors in the true HLOS winds and HLOS winds with additional errors. These error profiles are denoted ε_o and error correlations are computed using the well-known equation

$$\rho_{ij} = \frac{\langle \varepsilon_o(i) \varepsilon_o(j) \rangle}{\sqrt{\langle \varepsilon_o^2(i) \rangle \langle \varepsilon_o^2(j) \rangle}},$$

with brackets denoting the expected value over a large number of realizations. Similarly, horizontal error correlation, i.e., for two wind observation profiles a multiple of 200 km separated, we will compute horizontal error correlation by applying this equation on different vertical levels.

2.1.4 Error structure analysis

Errors in the receiver gain are flow dependent and hence imply error correlation associated with flow structures. These errors are of great concern for the assimilation, since these may introduce erroneous structures in the analyses and thus in the subsequent forecasts. Here we provide some preliminary guidance of the error structure analysis to be performed in task 3.

In order to investigate simulated error characteristics for the database each wind observation, U_{obs} , is considered to be determined by a general transfer function of the true wind, U_{true} , and the assumed errors on the following form (task 1a)

$$U_{obs} = \varepsilon_{bias} + (1 + \varepsilon_{g1}) \cdot U_{true} + \varepsilon_{g2} \cdot U_{true}^2 + \varepsilon_{g3} \cdot U_{true}^3 \dots, \quad (17)$$

where ε_{bias} is a constant or flow-independently varying bias error and the ε_{gX} coefficients represent flow-dependent gain errors of power X . An example of (17) for which we assumed a normally distributed random bias error, ε_{bias} , with a mean value of -1 ms^{-1} and a variance value of $1 \text{ m}^2 \text{ s}^{-2}$, a constant linear gain error, ε_{g1} , of -3% and a constant quadric gain error, ε_{g2} , of -0.3% is shown in Fig. 2.

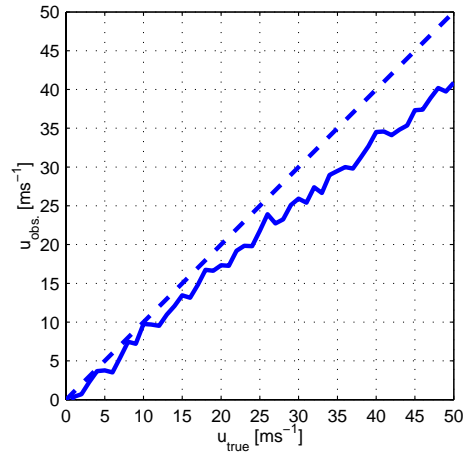


Figure 2. Schematic relation between the true, u_{true} (dashed line), and the observed, u_{obs} . (solid line), wind velocity. In this example a normally distributed random bias error, ε_{bias} , with a mean value of -1 ms^{-1} and a variance of $1 \text{ m}^2\text{s}^{-2}$, a constant linear gain error, ε_{g1} , of -3% and a constant quadric gain error, ε_{g2} , of -0.3% was assumed.

Different error characteristics were applied to the data set according to (17) and the threshold shear values were chosen such that large enough numbers of profiles and cross sections were extracted for the error statistics to converge. Figure 3 shows the mean and RMS errors integrated over all heights, as functions of the number of individual measurements. A constant linear gain error, ε_{g1} , of 1% was assumed. The data set shown here consists of rawinsonde data from the month of January for a period of three years (1995-1997) and is characterized by profiles holding values of shear exceeding $1.9 \cdot 10^{-2} \text{ s}^{-1}$. From the figure it is clear that the number of measurements required for the errors to converge to an accuracy of 3% is about 10^3 , i.e., \sqrt{n} , with $n = 1000$. In the case of the observations, the average number of measurements per sounding that pass the quality control (Håkansson 2001) is about 10, and consequently each subset requires $\sim 10^2$ soundings in order to describe accurate error statistics.

The height dependence of the error correlation was determined by storing error correlation values in height bins corresponding to the range gates of the ADM. In doing so, the mean height of each combination of pairs of measurements within a profile determines in which bin the error correlation value was to be stored. Range-gate averages of error correlation were then estimated. A similar approach was utilized for the determination of the dependence of the correlation on the vertical distance between measurements within a profile. For a given set of error coefficients, the error correlation may hence be considered a two-dimensional function of correlation mean height and correlation distance.

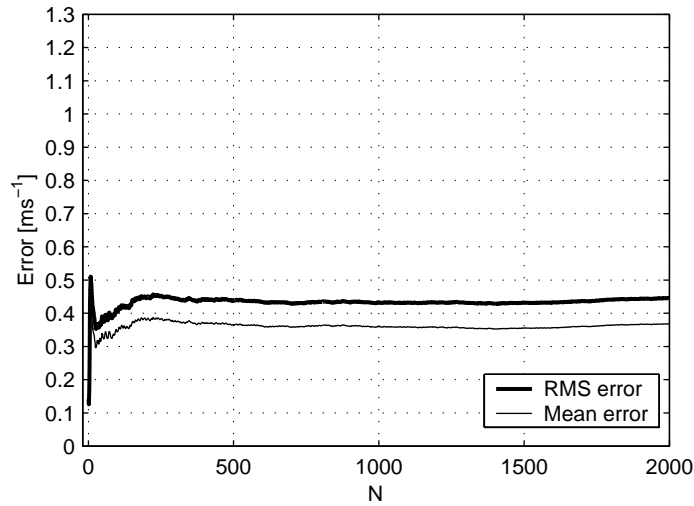


Figure 3. Mean and RMS errors as functions of sample size. A constant linear gain error, ε_{gl} , of 1% was assumed.

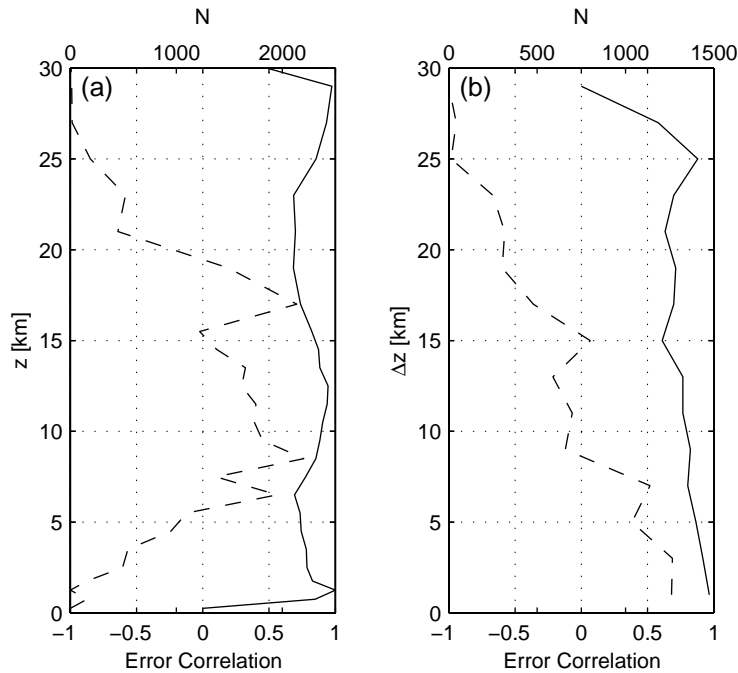


Figure 4. Error-correlation characteristics. (a) Vertical dependence. Mean error correlation (solid line) and number of observations for the respective height intervals (dashed line). (b) Dependence on distance between observations at heights between 8.5-13.5 km. Mean error correlation (solid line) and number of observations for the respective distance intervals (dashed line). A constant linear gain error, ε_{gl} , of 1% was assumed.

Error correlation characteristics for the set mentioned above are shown in Fig. 4. A constant linear gain error, ε_{gl} , of 1% was assumed. In Fig. 4 (a) the height dependence of the resulting error correlation and the distribution of correlated pairs are shown. The dependence of the correlation on the distance between two heights with a resolution of 2 km, together with the corresponding distribution of correlated pairs is displayed in Fig. 4 (b). The correlations of pairs with mean heights in the range 8.5-13.5 km are considered.

It is clear that under the assumption of an otherwise perfect instrument, even small gain errors will lead to significantly correlated wind observation errors. Under such circumstances error covariances contain more information as they provide measures of the magnitude of the error. In fact, the correlation between errors may be decreased were another independent gain or bias error to be included in the observation. The RMS error of the observation would however increase correspondingly. These effects are shown in Fig. 5 and 6.

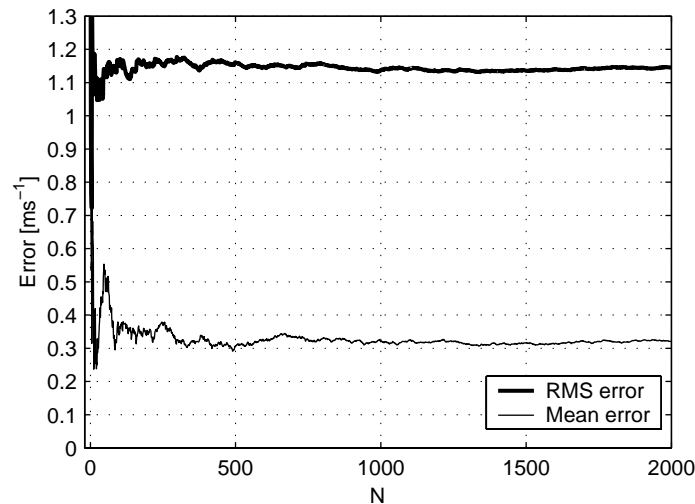


Figure 5. As in Fig. 3, although a normally distributed random bias error ε_{bias} with zero mean and a variance of $1m^2s^{-1}$ was also incorporated in the total error description.

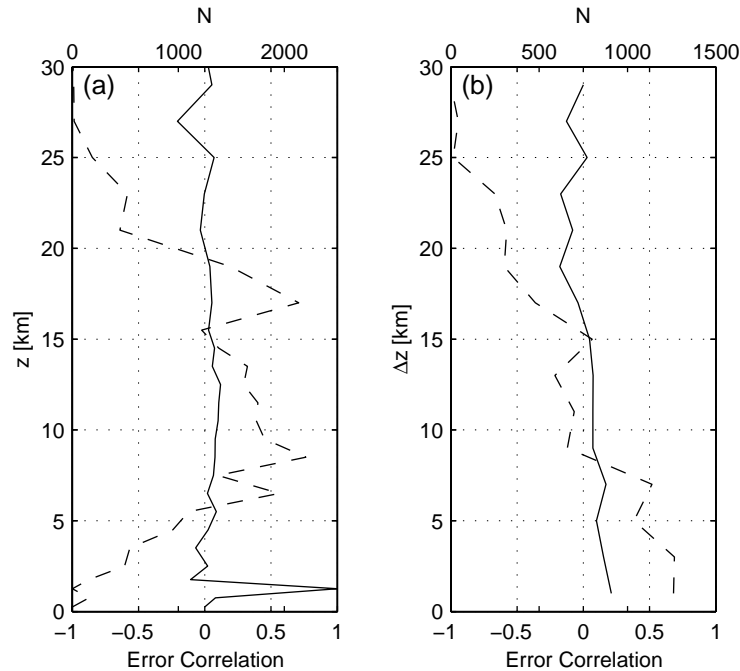


Figure 6. As in Fig. 4, although a normally distributed random bias error, ε_{bias} , with zero mean and a variance of $1\text{m}^2\text{s}^{-1}$ was also incorporated in the total error.

From Fig. 4 (a) it is clear that the error correlations assume values close to unity throughout the atmosphere when the errors are linearly dependent on the wind velocity alone. The flow dependence of the correlations is manifested as a weak “bulge” centered around ~ 12 km where the mean wind velocity, and hence the mean measurement error, have local maxima (Håkansson 2001). At $z=1.25$ km the correlation assumes the value of unity as there is only one pair of measurements representing that height. The negative slope of the correlation curve in Fig. 4 (b) implies that as the distance between two measurements increases, their mutual dependence decreases. Similar patterns appear, for the same reasons in Fig. 6, although the curves indicate much weaker correlations because of the inclusion of a random bias error.

2.2 Data Bases

Data bases of geophysical variables are needed, but are not always available. Here, we consider information on mesoscale wind variability and on aerosol distribution that help us define appropriate data bases for use in MERCI.

2.2.1 Mesoscale Wind Variability

A characteristic of the ADM is that each slant column of observations consists of the detected backscatter from a number (700) of laser shots. These shots/detections are performed during periods of about 7 seconds which, given the horizontal speed with which the satellite travels, correspond to horizontal distances of 50 km. The process is repeated every 200 km, the

observations thus represent 50-km averages of the HLOS winds separated by 200 km. In order to estimate the representativeness of such observed averages, a literature study on mesoscale wind variability has been performed.

Nastrom and Fritts (1992) and Fritts and Nastrom (1992) have investigated aircraft measurements of wind and temperature data collected during the Global Atmospheric Sampling Program (GASP) in search for sources of enhancement in mesoscale variability. Their attention was focused on estimating mesoscale variances and spectra over two lengths of flight segment, 64 and 256 km respectively, which make the study interesting for our purposes. All data were recorded with a horizontal resolution of ~ 1 km and at heights exceeding 6 km. It was shown that topographic features, jet streams, frontal and convective systems are primary sources for variability over both length scales. Extreme variances of the order $10 \text{ m}^2\text{s}^{-2}$ were occasionally encountered over marked topography and in the vicinity of jet streams and frontal zones (Fig. 7), whereas mean variances for these types of features were about $5 \text{ m}^2\text{s}^{-2}$ (Fig. 8). The observed variances correspond to variations in wind velocity which are in the range, or even exceed the required accuracy of the ADM. (The $2\text{-}3 \text{ ms}^{-1}$ accuracy required for the ADM corresponds to allowable variances in the range $4\text{-}9 \text{ m}^2\text{s}^{-2}$.)

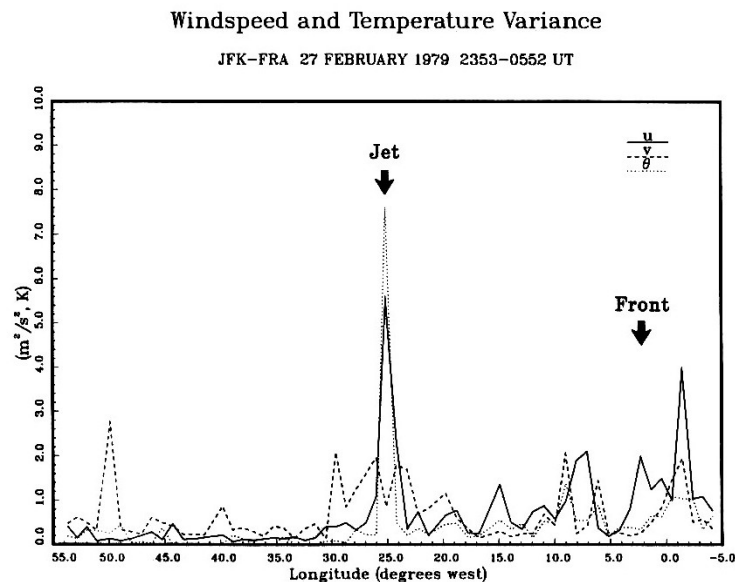


Figure 7. GASP observations showing 64 km variances of u , v and θ , taken from $\sim 54^\circ W$ to $5^\circ E$ on February 22, 1979. (From Fritts and Nastrom (1992).)

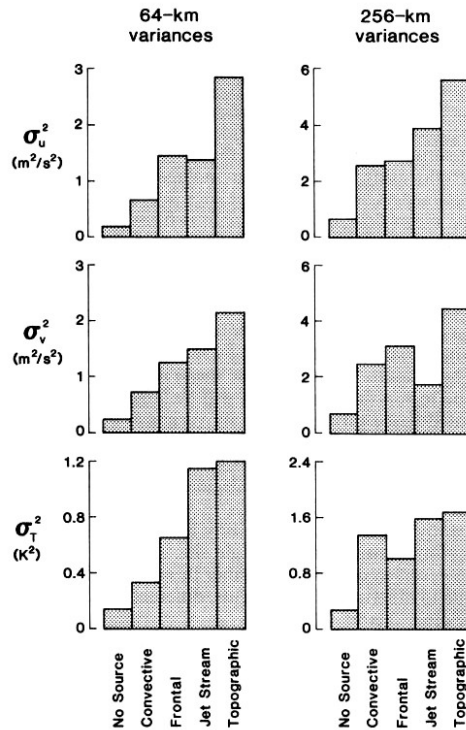


Figure 8. Mean variances of u , v and θ for various sources. (From Fritts and Nastrom (1992).)

The wind statistics study (Håkansson 2001) shows, considering the magnitude of the relative vorticity field and the horizontal integration length of the ADM, that in extreme cases an observation may be composed of measurements with a variability range of 50 ms^{-1} . It is also shown that the same range of variability may occur vertically within one range gate. It is clear that the ADM DWL can not provide meaningful observations in such cases. In fact, meteorological data assimilation systems usually reject observations in cases with extreme variability, since no useful representative interpretation of the observations in terms of analysis variables can be made (see eq. 16).

2.2.2 Influence of Humidity on Aerosol Scattering Properties

The response of the ADM is highly dependent on the atmospheric extinction of light, which in turn is a function of the aerosol distribution. It is thus of interest to study the performance of the instrument for realistic distributions of the aerosol field. However, collocated observed and modelled profiles of aerosol- and wind distributions are rare. Nevertheless, the characteristics of the aerosol field are to a significant degree determined by the presence of humidity in the atmosphere. The degree of hygroscopicity (Fig. 9) of the aerosol results in an increase in particle size and hence mass, given an increase in relative humidity, RH , which in turn leads to an enhancement of the aerosol's ability to extinct light. The increase in the extinction coefficient σ_e , generally implies enhanced aerosol scattering as determined by an increase of the scatter coefficient σ_{sp} .

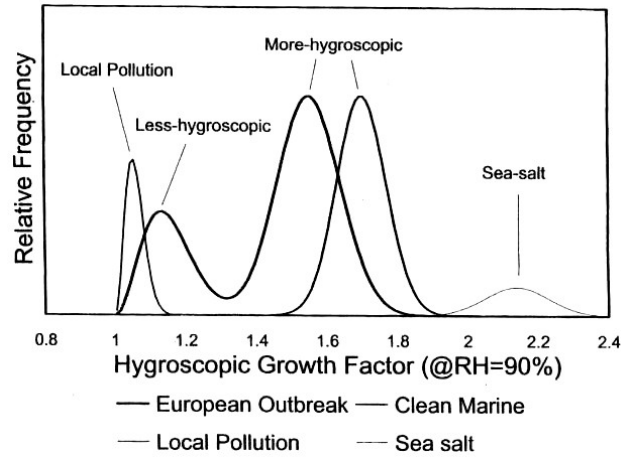


Figure 9. Schematic diagram of the sub-micrometer particle hygroscopic behaviour observed in clean air masses during the second Aerosol Characterization Experiment (ACE-2). The more-hygroscopic particle was observed at all times, whereas the concentrations of particles originating from local pollution and sea-spray varied considerably with time. (From Swietlicki *et al.* (2000).)

The dependence of σ_{sp} on RH is given by

$$\sigma_{sp}(RH) = \sigma_{spd} \cdot (1 - RH/100)^{-\gamma}, \quad (18)$$

where σ_{spd} is the scatter coefficient of the aerosol in a dry environment (Gassó *et al.* 2000). The dependence of σ_{sp} on RH is commonly displayed as the ratio $F(RH) = \sigma_{sp}(RH) / \sigma_{spd}$ (Ten Brink *et al.* 1996) from which the parameter γ may be determined by means of curve fitting (Fig. 10). Vertical profiles of γ were derived by Gassó *et al.* (2000), an example of which is shown in Fig. 11.

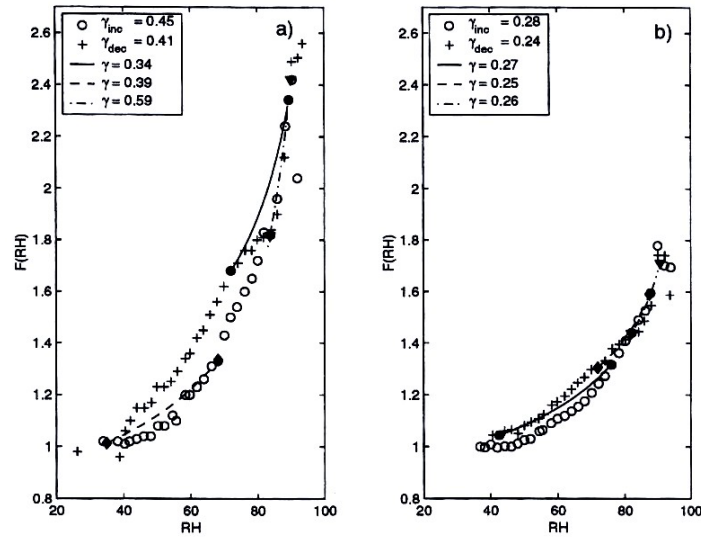


Figure 10. Plots of $F(RH)$ versus RH for (a) a clean marine air sample ($RH \sim 82\%$) taken during ACE-1 and (b) a polluted air sample ($RH = 75\%$) taken during ACE-2. The “O” and the “+” symbols respectively correspond to increasing and decreasing RH scans of the same aerosol sample. (From Gassó et al. (2000).)

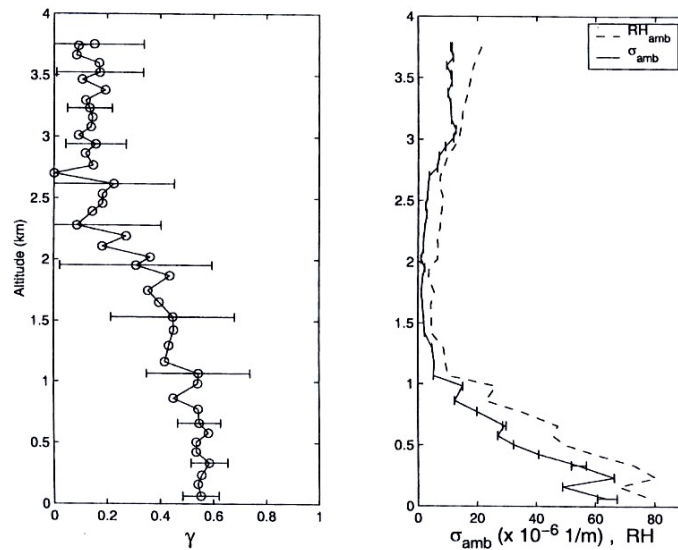


Figure 11. Vertical profiles of (a) γ and (b) derived ambient scatter coefficient, σ_{sp} ($\times 10^6 \text{ m}^{-1}$), and RH during ACE-2. (From Gassó et al. (2000).)

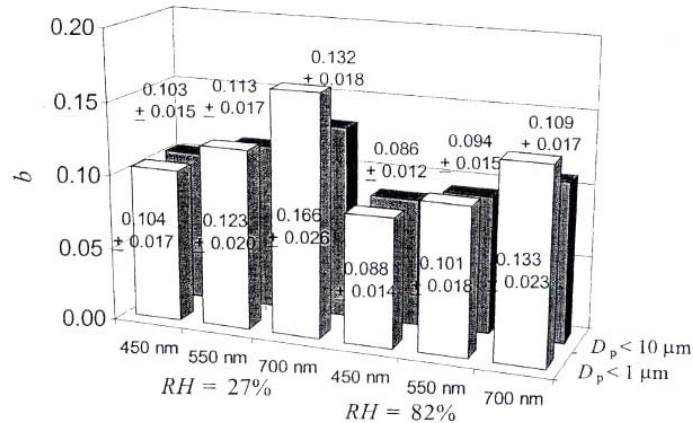


Figure 12. Hemispheric backscatter fraction $b = \sigma_{bsp} / \sigma_{sp}$ as a function of RH, particle size and wavelength for polluted periods during ACE-2. (From Carrico *et al.* (2000).)

From the figures it is clear that the humidity field has significant impact on the optical properties of the aerosol as the coefficient σ_{sp} at $RH \sim 90\%$ assumes values about 3 times that of σ_{spd} . The magnitude of the backscatter coefficient σ_{bsp} amounts to only about 10% of that of σ_{sp} (Carrico *et al.* 2000), however the relative impact of RH remains about the same (Fig. 12). While dependent on aerosol particle size distribution and the wavelength of the transmitted light, these effects only offset the variability of the aerosol's properties as determined by the humidity field.

On assuming realistic general particle size distributions of the aerosol, the relative humidity field as derived from observations and analyses, may be used in the simulation of effects of atmospheric extinction due to aerosol. One such realization is the frequently observed log-normal distribution (Quinn *et al.* 2000, Bates *et al.* 2000, Van Dingenen 2000, Collins *et al.* 2000, Flamant *et al.* 2000) exemplified in Fig. 13. The distribution may then be modified by the RH field to form a simulation of the aerosol effects in points collocated with those of the wind field. The resulting fields may serve as input to LIPAS. As the Rayleigh channel of the instrument measures molecular scatter, the assumptions should be utilized for the Mie channel only.

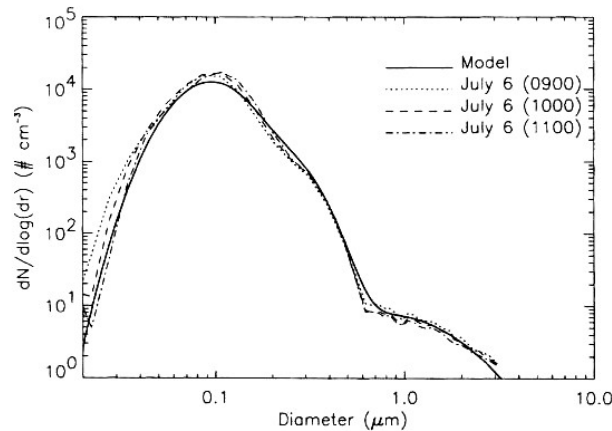


Figure 13. Particle size distribution in the marine atmospheric boundary layer as measured by various ship-mount instruments. Solid line corresponds to the best fit obtained with a modeled size distribution. (From Flamant *et al.* (2000).)

It is of importance to keep in mind that the variability in aerosol distribution may however be different from that of *RH*, for example in the case of pollution- or Saharan dust episodes in which no significant correlation between the two fields is discernible (Schmid *et al.* 2000).

2.2.3 Data Base Construction

The LIPAS modifications and error analyses can be applied to e.g. *i*) the typical cases of interest in Task 1b, *ii*) interesting cases found in the MISU derived database on atmospheric wind statistics or *iii*) LITE data collocated with ECMWF analysis fields.

From the database consisting of radiosonde- and model data described in the wind statistics study (Håkansson 2001), subsets of profiles and vertical pole-to-pole cross sections have been extracted. Four different “seasons” where each season consists of data representative for a specific month, accumulated during three consecutive years (1995-1997) are considered. The respective months are: January, April, July and October. The objective with this approach is to capture possible seasonal characteristics within a significantly reduced data set.

The data set is to be used with LIPAS in order to evaluate the error correlation performance of the ADM. Wind shear is chosen as the parameter for separating “relevant” profiles and cross sections from “irrelevant” ones, thus further reducing the size of the data set. Only profiles and cross-sections for which the maximum or mean shear exceeds certain threshold values were extracted to form the subset. With the wind shear acting as a “separator”, we are confident to extract mainly profiles holding certain variability in the wind field, whereas “dull” profiles of nearly constant or no wind velocity are omitted.

The ECMWF fields contain wind, temperature, humidity, cloud liquid water, and cloud cover information, which can serve as input for LIPAS. Over the selected profiles with large wind variability, the nominal ADM profiles will be simulated every 200 km, after which it will be

interesting to simulate ADM over the same profiles with some nasty errors, and analyse (subjectively) the potential for deformation or loss of critical wind structures.

2.3 Error Scenarii

Task 1a resulted in a sheer infinite number of possible error scenarii. In combination with results of task 1b and general data assimilation considerations, we here suggest a limited set of error scenarii.

2.3.1 Error Covariances

Not all error covariances are suitable for simulation in MERCI. In particular the more complex errors should be evaluated:

- Errors that can be directly specified as a wind error covariance can be assessed without further simulation by relating it directly to the conclusions of Task 1b;
- Errors that depend on t or I need to be simulated to assess their potential detriment by computing the spatial covariance structure over a given data set; We note that for 10 independent random wind difference samples of NWP model minus DWL per profile, and if assuming independent random errors on different profiles, then for an expected wind difference $\langle \text{NWP-DWL} \rangle = 3 \text{ m/s}$, 10 profiles can provide a bias correction with accuracy of about 0.3 m/s;

Clearly, the NWP model provides a reference that is useful for bias correction or quality monitoring, as is common practise for satellite data these days. Note however that on the synoptic scales no correction of systematic biases will be possible due to the limited number of samples available. As such, we study the covariance structure and distinguish by different time scale and different meteorological implication:

- Horizontal correlations and variances; most damaging on synoptic time scales 200-2000 km;
- Vertical correlations and variances; most damaging on all vertical scales 2-20 km.

In addition, combined vertical and horizontal covariance structures will be studied for some of the special cases as referred to in Task 1b.

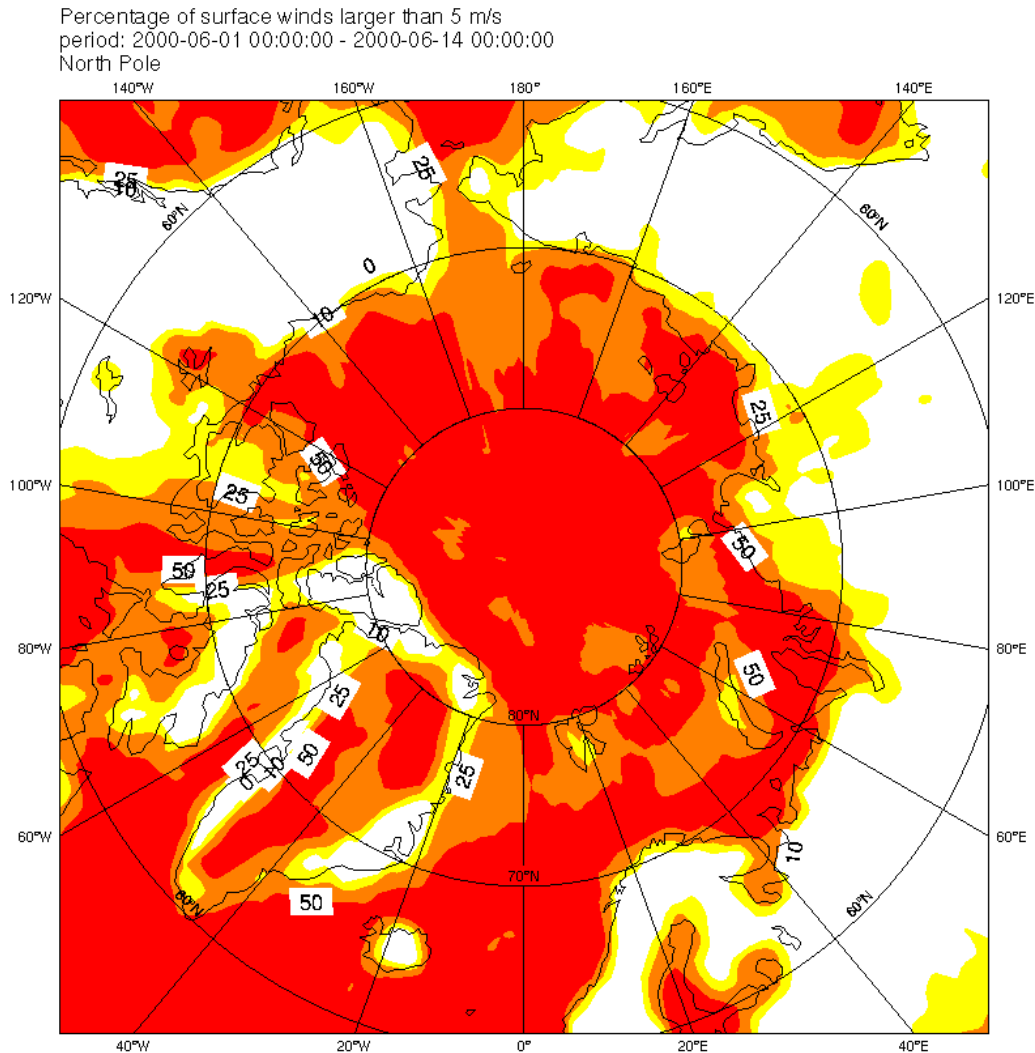


Figure 14. Percentage of surface winds larger than 5 m/s over the North Pole area in the summer period from 1-12 June 2000 according to ECMWF analyses. A high percentage of calm winds exists near steep orography and over land areas.

2.3.2 Wind Calibration

Poor wind calibration may obviously cause error on different time and space scales. However, geophysical external calibration sources, i.e., sources of opportunity, exist that reduce the need for an absolute calibration:

- Assimilation of wind shear observations, e.g., deduced from frequency shift differences $\Delta f(z=1) - \Delta f(z=j)$, may be considered rather than profiles of wind observations. This results in a loss of one range gate level of information per profile, since this is used as

geophysical reference. Note that the wind shear profile should not exhibit any further vertical or horizontal error correlations.

- Ground calibration over calm sea, land or ice areas. Figure 14 shows frequent occasions of calm winds in white and yellow. Unfortunately, in many locations over sea and ice, we will have in most cases winds above 5 m/s. Note however, that not many ideal cases may be needed along an orbit, while many profiles will be made. Over water, calm cases with currents or long waves may not be suitable, but these may be predictable. Anyway, over land calm targets seem more likely than over sea or ice, but here height variations are more frequent.
- In order to reduce the atmospheric contamination of the ground calibration range gate, the length of the lowest range gate may be reduced. However, effectively this would also result in the loss of a vertical level and thus in a loss of one piece of information in the vertical (see also first bullet).
- If biases are **stable** over many profiles, we can estimate $\langle \text{NWP-HLOS} \rangle$ for calibration as was mentioned in previous section.

2.3.3 Temperature Effects

The temperature of the atmosphere determines the bandwidth of Brownian motion of molecules. This dependency is known and may be tabulated in a response table (e.g., M. Endemann), which is a rather smooth (linear) function. Subtle effects, like Brillouin scattering, may complicate the theoretical expectations, but empirical tuning will be possible for a known temperature dependency. Moreover, if the Molecular channel atmospheric Doppler frequency shift can be expressed as

$$\Delta f = \text{GMF}(u,v,T)$$

where u,v , and T represent respectively the atmospheric variables of horizontal wind components and temperature, then we can compute from the NWP model state, which includes u,v , and T , an equivalent of Δf , and subsequently an observation innovation by taking the difference. By projection of this innovation back onto the NWP model state, through the analysis equations, we have effectively exploited the observation. In fact, one could say that not only the wind field, but also the temperature field, may be updated by ADM Doppler shift observations. Uncertainty in temperature dependency thus seems not problematic.

2.3.4 Proposed Error Scenarii

We foresee the following error scenarii as most relevant for study in MERCI:

- Atmospheric β heterogenities and clouds will be studied with LITE and collocated ECMWF data (KNMI);

- Vertical sub-range-gate wind variability, and β heterogeneities derived from q to be studied with sondes (MISU) to complement the KNMI studies with the coarser resolution ECMWF wind data;
- Vertical shift $\Delta z = 100$ m and $\Delta z = -100$ m due to range gate localisation errors;
- Rx gain bias $\alpha = \{-5\%, -1\%, 1\%, 5\%\}$; percentual biases present flow dependency;
- Rx gain bias $(\alpha_M, \alpha_R) = (-5\%, +5\%)$; inconsistencies between the Mie and Rayleigh channels could potentially cause serious wind shear observation errors;
- Combination of errors, in particular height and gain errors;
- Besides Rx gain errors, task 1a alluded to effects of higher order. We plan to take the expected frequency shift response function of the molecular receiver chain, which also includes a quadratic dependency on Doppler frequency shift, and change it by the percentages in Rx receiver gain bias mentioned above. As such, quadratic error terms, in addition to linear ones, will be studied.

3 Conclusions

The output of task 1 and the LIPAS software is used to define how to investigate variations of instrument parameter vector \mathbf{I} for sets of atmospheric states \mathbf{t} .

The lidar performance analysis tool (LIPAS), developed for ESA, will serve as the basis for simulating error correlation in HLOS wind observations. LIPAS includes incoherent detection at $0.355 \mu\text{m}$ laser wavelength and comprises i) returned signal intensity from atmospheric aerosols, molecules and earth radiance background; ii) characteristics of Fabry-Perot and Fizeau interferometers; iii) blocking filters; iv) CCD noise simulation; v) post-processing of the Mie multi-channel receiver and the Rayleigh dual-channel receiver. The output is a HLOS error profile for an accumulation of 0.5 sec. As such the parameter vector \mathbf{I} is represented in LIPAS. We defined modifications of this \mathbf{I} in order to simulate relevant observation error models, including error correlation. Ways to analyse the error correlation structure statistically or more subjectively in some critical cases are presented.

From task 1 conditions are specified where certain error conditions are expected. In this subtask we identify a meteorological database to perform simulations. However, combined mesoscale atmospheric wind, aerosol, and cloud conditions are not widely available. We propose to use:

Results from the project LITE4ADM, where LITE data are used at 355 nm to construct highly-resolved molecular, aerosol, and cloud backscatter profiles. These profiles are collocated with numerical weather prediction fields from ECMWF to provide wind and humidity information. The humidity information will be correlated with the LITE aerosol backscatter in order to estimate the usefulness of humidity as a tracer for aerosol loading.

Identify database for winds and relative humidity on observed scales from TEMP/PILOT measurements. Relative humidity will be used as a tracer for aerosol profile data. To this end, for a given set of TEMP/PILOT, distributions of humidity will be computed at each vertical level, that will be mapped on the LIPAS distributions of aerosol backscatter on the same level.

Extend the literature search for mesoscale variability (<50 km) with respect to Lorenc et al (1992) by incorporating more recent publications, including investigations on remote wind sensing systems (e.g., Gavrilov and Fukao, 1999; Hall, 1989; May et al, 1995; Nastrom and Fritts, 1992; Thuillier, 1995).

From the results of the wind statistics study, we identify a set of cases that can be used to evaluate the error correlation performance of the instrument simulator. We envisage sets of cross-sections with characteristic wind variability. Sufficient cases are selected in each set to test both the performance of the instrument in difficult situations and to test that the instrument meets the requirements as specified in subtask 1b. We envisage that part of the database may be used by the industrial team to test performance.

We identified a set of error scenarii that are trivial to analyse and therefore not so useful for statistical assessment:

- Profile biases, e.g. due to poor calibration and yaw off-set. Such biases, if they occur, obviously cause horizontal error covariances to be correlated; and affect all vertical levels in the same way. Biases that are constant in height can be eliminated by assimilating wind shear information. In this case one vertical level is lost (since it is used for reference);
- Errors that are repetitive and can be estimated by comparison to a reference data set, e.g. a NWP model.

Last but not least, we identified a minimum set of error scenarii that will be further evaluated in MERCI tasks 3 and 4.

4 References

- Bates, T. S., P. K. Quinn, D. S. Covert, D. J. Coffman, J. E. Johnson and A. Wiedensohler, 2000: Aerosol Physical Properties and Processes in the Lower Marine Boundary Layer: a Comparison of Shipboard Sub-Micron Data from ACE-1 and ACE-2. *Tellus*, **52B**, 258-272.
- Carrico, C. M., M. J. Rood, J. A. Ogren, C. Neusüß, A. Wiedensohler and J. Heintzenberg, 2000: Aerosol Optical Properties at Sagres, Portugal during ACE-2., *Tellus*, **52B**, 694-715.
- Collins, D. R., H. H. Jonsson, J. H. Seinfeld, R. C. Flagan, S. Gassó, D. A. Hegg, P. B. Russel, B. Schmid, J. M. Livingston, E. Öström, K. J. Noone, L. M. Russel and J. P. Putaud, 2000: In Situ Aerosol-Size Distributions and Clear-Column Radiative Closure During ACE-2. *Tellus*, **52B**, 498-525.
- Courtier et al, The ECMWF Implementation of Three Dimensional Variational Assimilation (3D-Var). Part I: Formulation, Quart. J. Royal Meteorol. Soc. 124, 1783-1808, 1998.
- ESA, "The Nine Candidate Earth Explorer Missions: Atmospheric Dynamics Mission", ESA SP1196(4), ESA/ESTEC, Noordwijk, the Netherlands, 1996.

- European Space Agency, Atmospheric Dynamics Mission. The four candidate earth explorer missions. Report for mission selection: ESA SP-1233(4) , 1999
- Flamant, C., J. Pelon, P. Chazette, V. Trouillet, P. K. Quinn, R. Froulin, D. Bruneau, J. F. Leon, T. Bates, J Johnson and J. Livingston, 2000: Airborne Lidar Measurements of Aerosol Spatial Distribution and Optical Properties over the Atlantic Ocean during a European Pollution Outbreak of ACE-2. *Tellus*, **52B**, 662-677.
- Flamant, P. H. and J. M. Vaughan, 2001: The Impact of Measurement Errors and Their Correlation on the Atmospheric Dynamics Mission. Review of the Requirement and ALADIN Concept. Task Note 1a: Review of the Potential Observation Error Correlation. ESA Reference FS/xxxx/PI/pi.
- Fritts, D. C. and G. D. Nastrom, 1992: Sources of Mesoscale Variability of Gravity Waves. Part II: Frontal, Convective, and Jet Stream Excitation. *J. Atmos. Sci.*, **49**, 111-127.
- Gassó, S., D. A. Hegg, D. S. Covert, D. Collins, K. J. Noone, E. Öström, B. Schmid, P. B. Russel, J. M Livingston, P. A. Durkee and H. Jonsson, 2000: Influence of Humidity on the Aerosol Scattering Coefficient and its Effect on the Upwelling Radiance during ACE-2. *Tellus*, **52 B**, 546-567.
- Gavrilov, N. M., S. Fukao, 1999: A Comparison of Seasonal Variations of Gravity Wave Intensity Observed by the MU RADAR with a Theoretical Model. *J. Atmos. Sci.*, **56**, 3485-3494.
- Håkansson, M., 2001. Determination of Atmospheric Wind Statistics, ESA report. ESA Contract No. 14659/00/NL/SF.
- Hall, F. F., 1989: Wind Variability Measured by Doppler LIDAR. *J. App. Met.*, **28**, 155-158.
- Hollingsworth, A., and P. Lönnberg, "The Statistical Structure of Short Range Forecast Errors as Determined from Radiosonde Data. Part I: The Wind Field", *Tellus* 38A, 111-136, 1986.
- Järvinen, H., E. Andersson, and F. Bouttier, 1999, Variational assimilation of time sequences of surface observations with serially correlated errors, *Tellus* 51A, 469-488.
- Liu, Zhi-Quan, and Florence Rabier (2001) about "Interactions between model resolution, observation resolution and density in data assimilation: One-dimensional study" (Paper submitted to QJRMS).
- Lorenc, A. C., R. J. Graham, I. Dharssi, B. Mcpherson, N. B. Ingleby and R.W. Lannon, "Study of preparation for the use of Doppler Wind Lidar information in meteorological assimilation systems", Final report on ESA study contract 9063/90.HGE-I, published by U. K. Meteorol. Office, Bracknell, England, 1992.
- Lorenc, A.C. , "Optimal Non-Linear Objective Analysis", *Q. J. R. Meteorol. Soc.*, **114**, 205-240, 1986.
- May, P. T., W. L. Ecklund, G. D. Hess, 1995: Spectral and Bispectral Characteristics of Wind variability at Darwin, Australia Observed by a VHF RADAR Wind Profiler. *Quart. J. R. Met. Soc.*, **121**, 527-544.
- Nastrom, G. D., D. C. Fritts, 1992: Sources of Mesoscale Variability of Gravity-Waves. 1. Topographic Excitation. *J. Atmos. Sci.*, **49**, 101-110.
- Quinn, P. K., T. S. Bates, D. J. Coffman, T. L. Miller, J. E. Johnson, D. S. Covert, J.-P. Putaud, C. Neusüß and T. Novakov, 2000: A Comparison of Aerosol Chemical and Optical Properties from the 1st and 2nd Aerosol Characterization Experiments. *Tellus*, **52B**, 239-257.
- Schmid B., J. M. Livingston, P. B. Russel, P. A. Durkee, H. H. Jonsson, D. R. Collins, R. C. Flagan, J. H. Seinfeld, S. Gassó, D. A. Hegg, E. Öström, K. J. Noone, E. J. Welton, K. J. Voss, H. R. Gordon, P. Formenti and M. O. Andreae, 2000: Clear-Sky Closure Studies of Lower Tropospheric Aerosol and Water Vapor during ACE-2 Using Airborne Sunphotometer, Airborne In-Situ, Space-Borne, and Ground-Based Measurements. *Tellus*, **52B**, 568-593.
- Statement of Work, " The Impact of Measurement Errors and their Correlation on the Atmospheric Dynamics Mission (ADM-Aeolus)", ESA, FS/0304/PI/pi, 2000.
- Stoffelen, Ad, 1998, thesis, <http://pablo.ubu.ruu.nl/~proefsch/01840669/inhoud.htm>.

-
- Stoffelen et al, 1994, Theoretical Studies of the Impact of Doppler Wind Lidar Data - Preparation of a data base, ESA-CR(P)-3943.
- Ten Brink, H. M., J. P. Veefkind, A. Waijers-Ijpelaan and J. C. van der Hage, 1996: Aerosol Light-Scattering in the Netherlands. *Atmos. Environ.*, **30**, 4251-4261.
- Thuillier, R. H., 1995: The Influence of Instrumentation, Siting, Exposure Height, and Temporal Averaging Methodology on Meteorological Measurements from SJVAQS/AUSPEX. *J. Atmos. Sci.*, **34**, 1815-1823.
- Van Dingenen, R., A. O. Virkkula, F. Raes, T. S. Bates and A. Weidensohler, 2000: A Simple Non-Linear Analytical Relationship between Aerosol Accumulation Number and Sub-Micron Volume, Explaining their Observed Ratio in the Clean and Polluted Marine Boundary Layer. *Tellus*, **52B**, 439-451.
- Vaughan, N.J. Geddes, P.H. Flamant, C Flesia, 1998, Establishment of a backscatter coefficient and atmospheric database, ESA-CR12510.
- Veldman, S.M, H.A. Knobbout, A. Stoffelen, G.J. Marseille and E.A. Kuijpers, 1999, LIPAS, executive summary, ESA, 3-9132/97
- World Meteorological Organisation, "Preliminary Statement of Guidance Regarding How Well Satellite Capabilities Meet WMO User Requirements in Several Application Areas". WMO satellite reports SAT-21. *WMO/TD No 913*, 1998.
- World Meteorological Organisation, "Guide to Meteorological Instruments and Methods of Observation", 6th edition, *WMO-No.8*, Secretariat of the World Meteorological Organisation, Geneva, Switzerland, 1996.

Acronyms

ADM	Atmospheric Dynamics Mission
ALADIN	Atmospheric Laser Doppler Instrument
AMI	Active Microwave Instrumentation on ERS
ATOVs	Advanced TOVS
CCD	Charge-Coupled Device
CLW	Cloud Liquid Water
CNRS	French national centre for scientific research
DNMI	Norwegian Meteorological Institute
DWL	Doppler Wind Lidar
ECMWF	European Centre for Medium-range Weather Forecasting
EPS	EuMetSat Polar System
ERS	European Remote-sensing Satellite
ESTEC	European Space research and Technology Centre
ESA	European Space Agency
EuMetSat	European organisation for the exploitation of Meteorological Satellites
GCOS	Global Climate Observing System
GOS	Global Observing System (meteorological)
HLOS	Horizontal LOS
HRPT	High Rate Picture Transmission
KNMI	Royal Netherlands Meteorological Institute
LIDAR	Light Detection and Ranging
LITE	Lidar In-space Technology Experiment
LIPAS	Lidar Performance Analysis Simulator
LMD	Laboratoire Meteorology Dynamique
LOS	Line Of Sight
MF	Meteo France
MISU	Department of Meteorology at Stockholm University
MMS	Matra Marconi Space (now Astrium)
NOAA	National Oceanic and Atmospheric Administration (USA)
NWP	Numerical Weather Prediction
OSE	Observation System Experiment
OSSE	Observation System Simulation Experiment
PBL	Planetary Boundary Layer of the atmosphere
PDUS	Picture Distribution System

PILOT	WMO code for conventional wind sounding
RfQ	Request For Quotation
SAF	Satellite Application Facility
SATOB	WMO code for satellite cloud-tracked wind
SMHI	Swedish Meteorological Institute
SoW	Statement of Work
TEMP	WMO code for conventional wind, temperature, and humidity sounding
TOVS	TIROS-N Operational Vertical Sounder
UV	Ultra Violet
WMO	World Meteorological Organisation
WP	Work Package